Eur. Phys. J. D **6**, 343–353 (1999)

THE EUROPEAN PHYSICAL JOURNAL D

EDP Sciences

Line mixing effects in the ν_3 band of CH_3F in helium: Experimental band shapes and ECS analysis

F. Thibault[1,a], J. Boissoles[1], I. M. Grigoriev[2], N. N. Filippov[2], and M. V. Tonkov[2]

[1] U.M.R. C.N.R.S. 6627, Université de Rennes I, Campus de Beaulieu, 35042 Rennes Cedex, France
[2] Institute of Physics, St. Petersburg University, Peterhof, 198904 St. Petersburg, Russia

Received: 27 October 1998

Abstract. Line mixing effects have been studied in the ν_3 band of CH_3F perturbed by helium. Theoretical absorption coefficients are compared to FTIR measurements, which were made at room temperature for helium pressure from 1 atm up to 90 atm. The observed strong modifications with respect to additive Lorentzian contributions are explained by line coupling effects. The Infinite Order Sudden Approximation and the Energy Corrected Sudden Approximation are used in order to account for these effects. The latter gives better agreement: it rather successfully predicts the band shape and the linewidths.

PACS. 33.20.Ea Infrared spectra – 33.70.-w Intensities and shapes of molecular spectral lines and bands – 34.10.+x General theories and models of atomic and molecular collisions and interactions (including statistical theories, transition state, stochastic and trajectory models, etc.)

1 Introduction

Modelling of line mixing in linear molecules has been described in many papers (see references [1,2] for a review). The case of CO_2 is the most extensively studied due to its atmospheric interest (see, for instance, references [3–5] and references therein). Considerably less work has been done on line mixing in spectra of non-linear molecules, for the following reasons. The treatment of line mixing uses parameters of the isolated lines such as position, width and intensity. However, the spectral studies, both experimental and theoretical, of "isolated line" parameters have mainly concentrated on line positions. The individual line intensities are less investigated; even for simpler molecules of atmospheric interest the distribution of line intensities is extrapolated from a limited set of measured values. Experimental studies of line broadening coefficients are also not very numerous for symmetric top molecules; see, for example, references [6–12]. Close coupling, or less accurate, theoretical pressure broadening cross-sections have also received not much interest [1,2, 12,13] owing to the increasing complexity for non-linear molecules. The latter is also true for rigorous modelling of the band shapes which is actually intractable for most non-linear molecules. Some research groups have therefore proposed various approaches in order to deal with line mixing manifestations at least qualitatively or semi-quantitatively. We may mention the semi-empirical model of Hartmann *et al.* [14] used for CO_2, CH_3Cl and CFC-22, the work of Rodrigues *et al.* [15] based on the Exponential Gap Law [1,2] applied for ozone mixed with O_2 and N_2, and the method of Tonkov *et al.* [16] proposed to simulate the band shapes of CO_2, O_3, CH_4 [16] and CH_3F [17]. In the latter, some linewidths were reported and more importantly a band shape analysis was proposed with the Adjusted Branch Coupling (ABC) method [16], which accounts for line mixing effects. The results of this work [17] stimulated us to perform a more extensive study.

From the viewpoint of the available data set, the case of the ν_3 parallel band of methyl fluoride seems to be favourable. The positions and intensities of the lines in this band have been obtained by Papousek *et al.* [18] and by Lepère *et al.* [19]. The authors also showed that the lack of directly measured data may be reasonably compensated by means of relatively simple extrapolations. Very recently, He-broadening coefficients were measured [11] in the ν_6 band of CH_3F and compared to semi-classical calculations based on the Robert-Bonamy [20] formalism. Several studies, both experimental and theoretical, done by De Lucia and co-workers, were devoted to the collision-induced transition rates and derived quantities such as pressure broadening cross-sections [21–24] (and references therein). Brechignac [13] in an original paper used the predictions of the Infinite Order Sudden Approximation (IOSA) [1,2] to explain the variation with pressure of the self-broadening parameter of the $R(1,1)$ IR line of the parallel band located at 2866 cm^{-1} under application of an electric field. This work however was limited to the dominant dipole-dipole interaction.

In view of the necessary approximations for a treatable relaxation model, the choice of the methyl fluoride

[a] e-mail: franck.thibault@univ-rennes1.fr

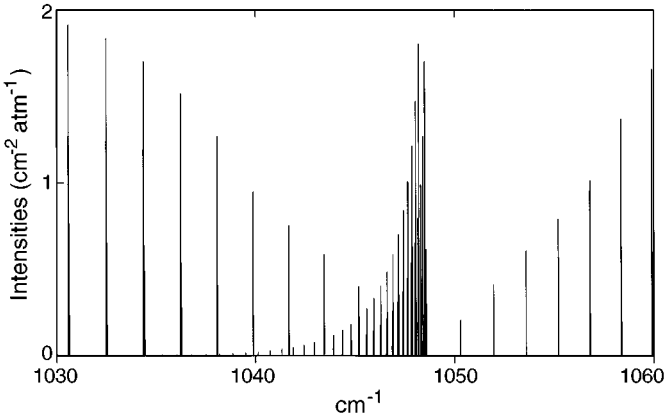

Fig. 1. Intensities of the lines in the central region of the ν_3 band of CH_3F. (Only the sub-bands with $K \leq 7$ are shown for clarity.)

molecule and of this very band also seems to be appropriate. The rotational constant $B \approx 0.85$ cm^{-1} is small enough to provide a dense energetic structure making valid reasonable approximations like IOSA. Nevertheless, it is sufficiently large for modern experimental techniques to allow measurements with various extent of spectral structure resolution. It is convenient that this band looks like a superposition of perpendicular linear molecule bands, *e.g.*, like the ν_2 band of carbon dioxide. Figure 1 illustrates the structure of the ν_3 band around the Q branches where many lines are crowded together within a narrow interval (~ 5 cm^{-1}). The ν_3 band is also very weakly perturbed by Coriolis interaction, and the splitting of the $K = 3n$ levels has not been observed [18].

For these reasons, quantum-mechanical calculations based on the work of S. Green [25] are *a priori* feasible. It is not possible to perform an accurate *ab initio* calculation since, to our knowledge, the CH_3F-He intermolecular potential is not yet available in any form. Instead, we attempted to apply IOS and ECS scaling-fitting laws, having He-broadening coefficients at our disposal, thanks to the recent results of reference [11].

The present paper is thus devoted to an ECS [1,2] analysis of an extensive set of experimental spectral band shapes for the ν_3 band of methyl fluoride mixed with helium. It is well known that this formalism is the most efficient and the proper one when accurate calculations (Close Coupling or even Coupled States) are intractable. Indeed, it includes properly the angular momenta coupling between radiation, rotation (and vibration) and expresses the relaxation matrix for an atomic perturber in terms of basic rates.

The paper is organised as follows. In Section 2 the experimental set-up and the methods of data treatment are reported. We recall the principles of the ECS frame in Section 3, and we underline the approximations made in the case of this system to obtain the band shape, the theory of which is given in Section 4. Results are presented and discussed in Section 5.

2 Experiment and data treatment

For the experimental studies we used the set-up available at the University of Rennes [26] with a Bruker IFS 120 HR Fourier transform spectrometer as a spectral instrument. We used a globar as a light source, Ge/KBr beamsplitter, MCT detector (HgCdTe at 77 °K), and a set of Oriel interference spectral filters. Commercially available methyl fluoride (Fluorochem Limited) and helium (Air Liquide) were used for the composition of gaseous mixtures. The purity of the helium was spectroscopically tested, and no sign of additional bands was detected. The purity of the methyl fluoride sample is not stated by the manufacturer; for its analysis, we registered the spectrum of a sample at the pressure of several Torrs with the greatest spectral resolution available (0.002 cm^{-1}). In fact, we detected only some traces of the water vapour spectrum in the region of the ν_2 band of H_2O, which is far beyond the spectral interval in question. The same spectrum was used as a test of the spectrometer calibration. We found that the line positions coincided with the recommended values reported in reference [18] with an inaccuracy of less than 0.001 cm^{-1}.

We utilised two different absorption cells. The first one with a pathlength of 21.3 cm and equipped with KRS-5 windows, was used for the measurements at higher pressures (up to 90 bars). The other one was a multiple-pass cell (30 cm base) with ZnSe windows used at lower pressures (up to 20 bars).

The mixtures were composed in the same cell which was then used for measurements. First, a certain quantity of methyl fluoride was introduced, and its pressure was measured using Datametrics 590 capacitance manometer (0–1000 Torr, 3 scales). After evacuating the connecting tubing, the cell was filled with helium, and the total pressure was measured using an appropriate manometer (Datametrics 590 for 1 bar, 1–10 bars and 10–50 FGP pressure gauges or Heise manometer 0–100 bars, precision 0.1% at full scale). To minimise a possible influence by CH_3F self-broadening on the registered spectral profiles, we used mixtures with relative absorber/perturber concentrations of 1:300 or less. We estimated that in this case the inaccuracy due to self-broadening does not exceed 2%, and it may be seen only in a region of the lowest measured values of the absorption coefficient.

We chose the spectral resolution with a four-point Blackman-Harris apodization function to register absorption shapes at any given pressure with minimal instrumental distortion. Roughly, the resolved spectral interval should be at least five times smaller than the FWHM of a line which may appear in the spectrum. The number of scans was chosen in order to optimise the signal-to-noise ratio in the measured absorbance spectrum $A(\sigma) = \log(I_0(\sigma)/I(\sigma))$, where $I(\sigma)$ is the sample spectrum and $I_0(\sigma)$ is the reference one, that is the spectrum of the cell filled with helium at the same pressure as used for the sample spectrum. Typically, the value of the standard deviation in a spectrum profile was about 0.001 of absorbance units. Indeed, the time of acquisition varied from some minutes to several hours.

Table 1. Absorption spectra of methyl fluoride mixed with helium: experimental conditions.

Total pressure (bars)	1	5	10	20	40	90
Initial pressure of CH_3F (Torr)	2.5	12.5	25	50	100	250
Temperature (°C)	27 ± 1	25 ± 1	25 ± 1	27 ± 1	27 ± 1	27 ± 1
Scans per spectrum	500	400	400	400	40	40
Spectral resolution (cm^{-1})	0.022	0.043	0.055	0.11	0.3	0.3
Number of spectra for averaging	7	7	8	12	6	6
Optical pathlength (cm)	615	975	975	975	21.3	21.3

All studies were performed at room temperature. The temperature was measured by a platinum resistance thermometer attached to the body of the cell which was placed in the evacuated cell compartment of the spectrometer. The stability of the temperature was maintained by a system of air conditioning, and the temperature was monitored during the whole time of recording. Some essential parameters of recordings are given in Table 1.

To study the line mixing effects, it is essential to measure the absorption band shape in the widest possible interval of the absorption coefficient. The reason for this is that the most sensible intervals for line mixing are usually those with maximum (Q branch) and minimum (band wings) intensities. We used the method of "complete absorption profile" described in more detail in reference [17].

It is worth noting that this method is applicable if the band shape does not depend on the absorber concentration; which is the case for the chosen band. It is also true that the eventual baseline variation should be carefully controlled. To overcome the latter problem, we studied in advance the stability of the reference spectrum which was found to be satisfactory, that is, with no spectral peculiarities. For each series, we registered one reference spectrum before the sample spectra and another one after it. Their ratio was used as a test of the baseline stability for a given series. The spectral interval of registration was chosen as wide as possible to observe spectral intervals with no significant absorption at any concentration of methyl fluoride (so-called "points of transparency"). For example, the spectra at higher pressures were recorded in the spectral interval of 800–1900 cm^{-1}. This allowed the baseline to be controlled at two points of transparency, namely, at 900 cm^{-1} and at 1700 cm^{-1}. The variations of the baseline proved to be not very great but measurable, taking into account the achieved standard deviation of absorbance of the order of 0.001. The absorbance level at the points of transparency varied less than 0.03 absorbance units, and the slope of baseline never exceeded 0.02 absorbance units over the total interval of registration. The baseline was corrected for each spectrum before its further treatment.

We believe that after baseline corrections the main source of inaccuracy in the absorption coefficient is the uncertainty of the initial concentration of methyl fluoride in the mixture which may be of the order of 3-4 percent. The spectral profile seems to be measured more precisely; we estimate the band shape inaccuracy to be about 2% regardless of the absolute absorption value.

3 ECS Frame

3.1 Notations and approximations

As stated above, this work is based on the IOS approximation of Green [25] which is valid for a symmetric top rigid rotor (the active molecule) colliding with an atom (the perturber). In his work Green [25] had considered primitive and parity-adapted symmetric top functions. In the following we will keep the first set because the K-doubling (in the $K = 3n$ sub-bands) is not observed. Due to this and because the "umbrella" inversion is not possible for the molecule CH_3F, we cannot investigate the effects of propensity rules [27] for rotationally inelastic collisions.

To simplify notation, an infrared transition k between an initial level i and a final level f is written in the Liouville space: $|k\rangle\rangle = |\nu_i J_i K_i \nu_f J_f K_f\rangle\rangle$, where for instance ν_i stands for the complete set of vibrational quantum numbers (including vibrational angular momentum), J_i is the rotational quantum number, K_i its projection on the axis of symmetry. A similar notation holds for a line λ: $|\lambda\rangle\rangle = |\nu'_i J'_i K'_i \nu'_f J'_f K'_f\rangle\rangle$ coupled to the line k.

Since we deal with a non-degenerate vibration, namely the ν_3 band, which is expected to be uncoupled with other bands, and since we neglect vibrational inelasticity, we will omit the ν's.

The starting point of this frame [25] is the generalised IOS basic rates: $Q'(L, M_i, M_f; E)$, where L, M arise from the multipolar expansion of the intermolecular potential developed in spherical harmonics and where E is the relative kinetic energy of the collision. The L values vary from $J_i + J'_i$ (or $J_f + J'_f$) to $|J_i - J'_i|$ (or $|J_f - J'_f|$) and M_i (M_f) varying from $|K_i - K'_i|$ (respectively, $|K_f - K'_f|$) to $K_i + K'_i$ (respectively, $K_f + K'_f$) for collision-induced transitions between lines k and λ.

In fact, in CH_3F, two species coexist depending on the relative orientation of the nuclear spin of the three hydrogen atoms. Levels with $K = 3n$ (A symmetry) are designated ortho-CH_3F, and levels with $K = 3n \pm 1$ (E symmetry) are designated para-CH_3F. These two symmetry species do not readily interconvert, either radiatively

or collisionally; this can however occur via magnetic hyperfine interaction. Thus, we have a propensity rule for the rotational levels: $A \leftarrow | \rightarrow E$. One can thus consider the gas of active molecules as being composed of two independent species. Moreover, the $C_{3\nu}$ symmetry of CH_3F imposes a restriction that collisions may change the quantum number k (k is the signed value of K) only by a multiple of three: $\Delta k = 3n$. Schwendeman and coworkers [28] demonstrated by infrared-infrared double resonance that K-changing collisions are significant in this band of CH_3F.

The parallel ($\Delta K = 0$) ν_3 band of methyl fluoride is a superposition of K-sub-bands. To go further, we have assumed that the levels with different K values are not coupled via collisions. This assumption removes the collisionally allowed $\Delta K \neq 0$ transitions. The validity of this assumption is however not obvious [15,25,29]. Nonetheless, this might be a reasonable approximation for a prolate top with the rotational constant A much greater than B [30] and a small constant D_{JK}. Note also, following Oka [31], that, for example, transitions for $K = 4$ to $K = 5$ are expected to be very weak because, although these are para-transitions, a change of $\Delta k = 9$ is needed. Another argument may be found in our work [17], where we tested the ABC model for two cases, namely, with and without mixing of K components. The spectral band shapes proved to be insensitive to the extent of K coupling in the framework of the ABC model. Obviously, the absence of K coupling simplifies calculations, and the computing time diminishes drastically; the latter fact is rather important because the calculations can be performed in a reasonable time.

We are thus left with:

$$Q'(L;E) \equiv Q'(L,0,0;E) = Q'(L,M_i,M_f;E)\delta_{M_i 0}\delta_{M_f 0}. \quad (1)$$

3.2 Cross-sections

It had been shown [1,2,25] within the IOS approximation that the generalised IR cross-sections can be factored into spectroscopic and dynamical coefficients. The resulting equation for downward transitions ($J_i > J'_i$) is [3]

$$\sigma^1(k \rightarrow \lambda) = -\left(\frac{[J'_i]}{[J_i]}\right)^{1/2} \sum_L [L] F^{1K_iK_fL}_{J_iJ_fJ'_iJ'_f} Q'_L(T)\,, \quad (2)$$

with $K_f = K_i$, since we consider a parallel band, and $[X] = 2X + 1$. The spectroscopic coefficients F which take into account, through the familiar $3j$-$6j$ angular-momentum-coupling symbols, the coupling of the different angular momenta involved, are defined by

$$F^{1K_iK_fL}_{J_iJ_fJ'_iJ'_f} = -([J_i][J'_i][J_f][J'_f])^{1/2} \times \begin{pmatrix} J_i & L & J'_i \\ K_i & 0 & -K_i \end{pmatrix} \begin{pmatrix} J_f & L & J'_f \\ -K_f & 0 & K_f \end{pmatrix} \begin{Bmatrix} J_i & J_f & 1 \\ J'_f & J'_i & L \end{Bmatrix}. \quad (3)$$

It should be emphasised once more that we have set K'_i equal to K_i, which is the main simplification in the present work. The dynamical factors, or basic rates, $Q'_L(T)$ are actually the basic rates from equation (1) thermally averaged over kinetic energy according to the Maxwell-Boltzmann distribution:

$$Q'_L(T) = \frac{1}{(k_BT)^2} \int_0^\infty E e^{-E/k_BT} Q'(L;E)\mathrm{d}E\,. \quad (4)$$

They may be considered as inelastic cross-sections for downward transitions to the ground state within $K = 0$, namely, $\sigma^0(L \rightarrow 0;T)$. The cross-section for the reverse process, for $J_i < J'_i$, is given by the detailed balance principle:

$$\rho_k \sigma^1(k \rightarrow \lambda) = \rho_\lambda \sigma^1(\lambda \rightarrow k)\,, \quad (5)$$

where the ρ's are the populations of the initial level of the radiative transition.

The IOSA is known to be rather accurate, especially when the rotational spacing is small compared to the thermal energy. It is certainly true for the molecule of CH_3F at 296 K ($k_BT \approx 205$ cm^{-1}) considering the transitions which form the band in question. The ECS formalism attempts to put back into the calculations of the rates some of the adiabaticity removed in the IOSA [1,2] by the neglect of the rotational energy-level spacing and of the finite duration of the collision. This was done by De Pristo *et al.* [32] who introduced an additional factor $A(J,L)$ into the IOS scaling law to account for the rotation of the molecule during the collision. The "ECS-factor" of De Pristo *et al.* [32] can be written as follows:

$$A(J,L) = \frac{\sqrt{\Omega_{J_i}\Omega_{J_f}}}{\Omega_L} \quad (6)$$

and according [5] to the work of Bonamy *et al.* [33] the adiabaticity factor takes the form

$$\Omega_L = \left(1 + \frac{\lambda_c^2 \omega^2_{L,L-1}}{12\overline{v}^2}\right)^{-1}, \quad (7)$$

where $\omega_{L,L-1}$ is the difference in angular frequency between adjacent levels and λ_c is a scaling length. Consequently, the collisional time, $\lambda_c/\overline{v}$, is an additional parameter that is included in the ECS scaling law, where λ_c is understood to be an effective impact collision length and $\overline{v}$ is the average relative velocity.

The main quantities in these approximations that are still unknown are the basic rates. They were modelled through the simple analytical power law:

$$Q'_L(T) = \frac{A(T)}{[L(L+1)]^\alpha}\,, \quad (8)$$

where $A(T)$ and α are adjustable parameters.

Finally, let us recall that the cross-sections are purely real quantities, due to the use of equation (1). As a consequence, no rotational line shifts are predictable.

4 Line shape formulation

4.1 General formulation

We consider a mixture of radiatively active molecules a with a transparent buffer gas b with densities n_a and n_b at a temperature T. The absorption coefficient $\alpha(\sigma)$ accounting for line mixing within the impact and binary-collision approximations is given by [34–37]:

$$\alpha(\sigma) = n_a \frac{8\pi^3}{3hc}\sigma(1-\exp(-hc\sigma/k_{\rm B}T))\sum_{\nu}|R_\nu|^2 \times {\rm Im}\frac{1}{\pi}\sum_{k,\lambda} d_\lambda \langle\langle\lambda|(\sigma-\sigma_0-in_bW^0)^{-1}|k\rangle\rangle d_k\rho_k, \quad (9)$$

where d_k is the reduced dipole matrix element for line $|k\rangle\rangle$ and R_ν the vibrational dipole moment; σ, σ_0 and W^0 are operators in Liouville space, associated, respectively, with the scanning wavenumber, the line position, and the collisional process. σ and σ_0 are both diagonal and real, while W^0 is non-diagonal and in general complex (although real here: see above). The off-diagonal elements of the relaxation matrix W^0 account for line interference whereas the diagonal values are proportional to the broadening coefficients.

The matrix elements of W^0 are related to the IR cross-sections by

$$\langle\langle\lambda|W^0|k\rangle\rangle \equiv W^0_{\lambda k} = \frac{\overline{v}}{2\pi c}\sigma^1(k\rightarrow\lambda)\,. \quad (10)$$

In fact, in this formalism, diagonal elements have to be deduced from the sum rules [38,39]

$$W^0_{kk} = -\sum_{\lambda\neq k}\frac{d_\lambda}{d_k}W^0_{\lambda k}\,, \quad (11)$$

and it is well known [3–5,38] that any band shape modelling should respect these rules.

4.2 Spectroscopic details

Four bands of CH_3F were taken into account to calculate the spectra in the region 950–1100 cm^{-1}. These are the ν_3 and $2\nu_3 \leftarrow \nu_3$ bands of $^{12}CH_3F$ and $^{13}CH_3F$. Note that ECS calculations were performed only for the ν_3 band of the main isotopomer. The other band shapes were considered as being composed of individual Lorentz line shapes.

The intensity of an isolated line $|k\rangle\rangle$ at a temperature T is

$$S^0_k = \frac{S^0_\nu I_a \varepsilon_k}{Q_{\rm R}}\frac{\sigma_k}{\sigma_\nu}[1-\exp(-\beta hc\sigma_k)] \times \exp(-\beta hcE_{{\rm R}i})F(J_i)A(J_i,J_f,K_i)\,, \quad (12)$$

where $\beta = (k_{\rm B}T)^{-1}$, $E_{{\rm R}i}$ is the rotational energy of the initial level. Energy levels, band centre σ_ν and line positions σ_k were generated by means of the spectroscopic constants given by Papousek *et al.* [18]. The rotationless bandstrength of the ν_3 band was taken from reference [19], $S^0_\nu = 377.9\ {\rm cm}^{-2}\,{\rm atm}^{-1}$ at 296 K. The integrated intensity of the hot bands was deduced by multiplying the square of the vibrational dipole moment by two accounting for the vibrational level population. $Q_{\rm R}$ is the rotational partition function (for the ortho- or para-states), $Q_{\rm R} = 7217.4$ [19], I_a is the isotopic abundance of carbon, and ε_k is the spin-rotation statistical weight for a given J,K level: $\varepsilon_k = 4(2-\delta_{0,K})$ if $K = 3n$ including $n = 0$, $\varepsilon_k = 2(2-\delta_{0,K})$ otherwise. Finally, in this equation $F(J_i)$ is the Herman-Wallis factor and $A(J_i,J_f,K_i)$ is the Hönl-London factor.

All the lines of the K-sub-bands with K varying from 0 to 25 which have an intensity greater than $1\times10^{-6}\,{\rm cm}^{-2}{\rm atm}^{-1}$ have been considered. This represents more than 98% of the band intensity for the ν_3 band of the $^{12}CH_3F$.

4.3 Effective calculation

Within the framework of the two preceding sections, band profile calculations could be undertaken. Moreover, the matrix elements of the $(\sigma-\sigma_0-in_bW^0)^{-1}$ operator were calculated from the eigenvalues Λ_k and eigenvectors X of $(\sigma_0+in_bW^0)$ as outlined in references [34–37]:

$$\alpha(\sigma) = \frac{S^0_\nu P_a I_a}{Q_{\rm R}}\frac{\sigma}{\sigma_\nu}[1-\exp(-\beta hc\sigma)]\sum_K\varepsilon_K \times\frac{1}{\pi}\sum_k {\rm Re}(G_{kk})\frac{1}{[\sigma-{\rm Re}(\Lambda_k)]^2+[{\rm Im}(\Lambda_k)]^2} \times[{\rm Im}(\Lambda_k)+Y_k[\sigma-{\rm Re}(\Lambda_k)]] \quad (13)$$

with

$$G_{kk} = \sum_{jl}(X^{-1})_{kl}\rho_l d_j d_l X_{jk}\,, \quad (14)$$

and

$$Y_k = \frac{{\rm Im}(G_{kk})}{{\rm Re}(G_{kk})}\,, \quad (15)$$

$$\sum_k {\rm Im}(G_{kk}) = 0\,, \quad (16)$$

where X_{jk}, in equation (14), is a matrix whose columns are the normalised eigenvectors X.

The formula for the absorption coefficient takes into account line mixing effects. It appears from equation (13) that, whatever the amount of line overlap, the absorption coefficient can be expressed as a sum of effective lines characterised by intensities ${\rm Re}(G_{kk})$, wavenumber ${\rm Re}(\Lambda_k)$, and half-width ${\rm Im}(\Lambda_k)$. Each line k contributes to the band shape with a Lorentz profile and a dispersive profile that leads to an asymmetric line shape profile and redistributes its strength inside the band without modifying its integrated intensity (Eq. (16)) [40]. Y_k is the so-called line interference parameter associated with this phenomenon.

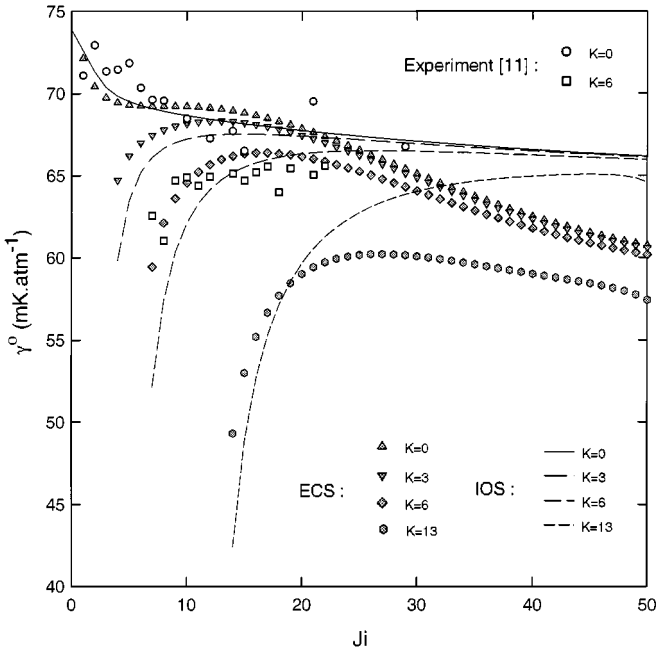

Fig. 2. Comparison between experimental, ECS and IOS half-widths (in $10^{-3}\,\mathrm{cm}^{-1}\,\mathrm{atm}^{-1}$ at 296 K) in various sub-bands.

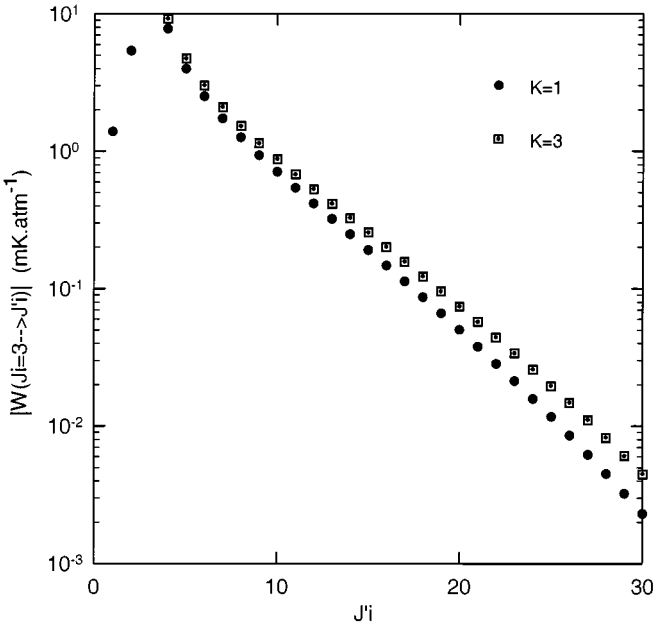

Fig. 3. Comparison of the relaxation matrix element coupling the line $Q(J_i = 3)$ to other lines Q in the sub-bands $K = 1$ and $K = 3$.

Table 2. ECS-P and IOS-P parameters.

	ECS	IOS
$A(\text{Å}^2)$	4.6225	10.085
α	0.80	1.075
$\lambda_c(\text{Å})$	2.0	0

It is worth noting that it is not a first-order one as derived by Rosenkranz [35] or Smith [37].

Let us remark that if one only keeps the diagonal elements (the linewidths) obtained via the sum rules, one recovers a band profile expressed as a summation of Lorentz line shapes whose parameters are taken from the same model. Apparently, it is often useful to calculate band deviation functions [38] that are the ratios of the band shape in question, either experimental or a model one, to the Lorentz sum profile mentioned above; this approach will be discussed in a forthcoming paper. To bring to the fore line mixing effects we should also compare the measured spectra with those derived as a sum of the usual Lorentz contours:

$$\alpha(\sigma) = \frac{P_a}{\pi} \sum_m \frac{\sigma[1-\exp(-\beta hc\sigma)]}{\sigma_m[1-\exp(-\beta hc\sigma_m)]} \times S_m^0 \frac{P_b\gamma_m^0}{[\sigma-\sigma_m]^2+[P_b\gamma_m^0]^2}\,, \quad (17)$$

where the pressures P_a and P_b may be simply recalculated from the corresponding densities n_a and n_b used in equation (9). The half-widths at half-maximum (HWHM) were maintained fixed for all the lines m at $\gamma_m^0 = 66.4 \times 10^{-3}\,\mathrm{cm}^{-1}$ per helium atmosphere at 296 K.

5 Results and discussion

In this section, predictions of the ECS formalism are compared with experimental linewidths and spectra. In the limit that the scaling length $\lambda_c = 0$, the ECS scaling law reduces to the IOS approximation (for downward rates).

The ECS-P (with P standing for the power scaling law, Eq. (8)) adjustable parameters A, α, and λ_c have been deduced a from least squares fit of experimental linewidths [11] by using the sum rules (Eq. (11)) along with three experimental points of the spectrum at 10 bars located at the top of the Q branches and in the troughs in the intermediate P-Q and Q-R regions. The helium broadening coefficients from reference [11] were measured in ${}^RQ_0$ and ${}^RQ_6$ branches of the ν_6 band of CH_3F. Comparing them with the estimations made in reference [17] for the ν_3 band, we supposed that there is no significant vibrational dependence of linewidths. So, we assumed them valid for the P branch of the $K = 0$ and the Q branch of the $K = 6$ sub-bands of the ν_3 band despite the different nature of these bands (ν_6 perpendicular, ν_3 parallel). The fitted parameters are given in Table 2. It should be noted that these parameters, especially A and α, are correlated. Due to the complexity of the ν_3 band it is not possible to decorrelate these parameters as this was done by simultaneously fitting the linewidths and the band wing of the $3\nu_3$ band of CO_2 in helium or in argon [5,41]. This is why the complete and statictically correct analysis of the inaccuracies of the obtained parameters was not performed.

The resulting value for the scaling length (cf. Table 2), $\lambda_c = 2$ Å, appears to be reasonable if compared to the usual collisional range, typically close to the Lennard-Jones diameter ($\sigma \approx 3$ Å [11]) or if compared to the value

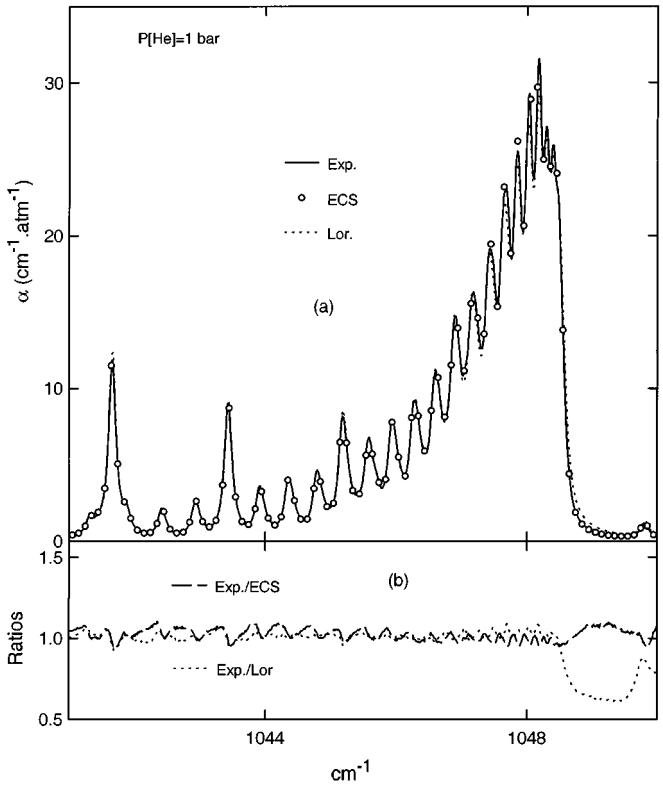

Fig. 4. Comparison between (a) the experimental spectrum (solid line) normalized per CH_3F atmosphere, the ECS calculation (open circles) and the Lorentzian calculation (dotted line) for helium pressure of 1 bar in the Q branches region and (b) the ratios of the experimental spectrum to the ECS calculation and to the Lorentzian profile.

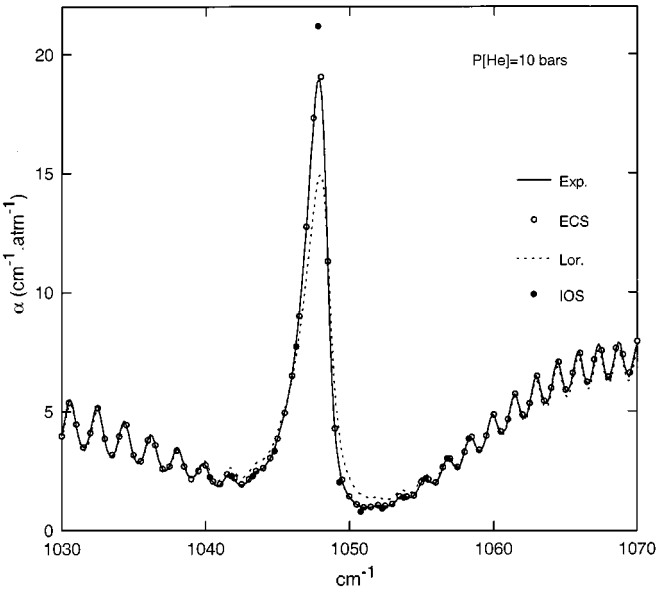

Fig. 5. Comparison between the absorption spectrum, the ECS model, the IOS model and the Lorentz band profile in the central region of the band at the helium pressure of 10 bars.

obtained in our previous studies for the cases of CO_2-He ($\lambda_c = 0.66$ Å [3]) and CO_2-Ar ($\lambda_c = 3.5$ Å [5]).

5.1 Linewidths

The agreement between the experimental linewidths and the corresponding calculated ones is satisfactory as shown in Figure 2. The decrease of the HWHM with J in the $K = 0$ sub-band is well reproduced; this effect has been observed for various molecules. The widths in the other sub-bands, that is for any given $K \neq 0$, increase with J if the values of K and J do not differ much, and they decrease at greater values of J. For a given J, the widths decrease as K increases. Similar regularities were observed for the ν_3 band of CH_3Cl with different perturbers [6,7], for the ν_3 band of CH_3D in O_2 [10] and even for NH_3 with O_2 [8]. Moreover, our calculations show that, at a given J, $\gamma^0(J,K)$ decreases with K more significantly at lower J than at higher ones; this was also noted in reference [9] for self-broadening coefficients of CH_3F. This trend with K at lower J values could be explained in a variety of ways. First, we assumed, in this study, the rule $\Delta K = 0$ for collision-induced transitions; apparently, they are the most probable ones. The value of K cannot be decreased by a collision, so when J is close to K, changes in J are not favoured since J cannot become less than K. Consequently, the number of relaxation channels is thus diminished. Second, we may consider relaxation matrix elements $W_{k\lambda}$ which decrease roughly exponentially with J: see Figure 3. The ECS linewidths are given by equation (11), that is by sum of non-diagonal matrix elements which comprises the elements with the same K (since $\Delta K = 0$) and various J for a given line. The greater the value of K, the fewer the number of significantly large matrix elements taken into account, as $J \geq K$. It therefore appears reasonable that, for instance, $\gamma_Q(3,3)$ is less than $\gamma_Q(3,1)$. Finally, this behaviour may be explained in view of the role of the anisotropic part of the repulsive intermolecular potential as in reference [11].

Are also shown in Figure 2 the IOS linewidths which reproduce the main trends. However, the IOS model leads to an independence of the line widths on J at higher J values. This is not surprising since the IOSA is not accurate at higher J values, and it is well known that the ECSA remedies this problem [42–44].

5.2 Band shapes

We first consider the spectrum recorded under atmospheric pressure of helium. Experimental and computed spectra are plotted in Figure 4a. Slight differences exist in the Q branches region between the Lorentzian spectrum and the ECS or the experimental ones. These differences are more pronounced in the trough near 1049 cm^{-1}: see Figure 4b. The ratio of the experimental spectrum to the Lorentz calculation plotted in Figure 4b shows that even for such a moderate pressure one should be cautious of using a Lorentz band shape.

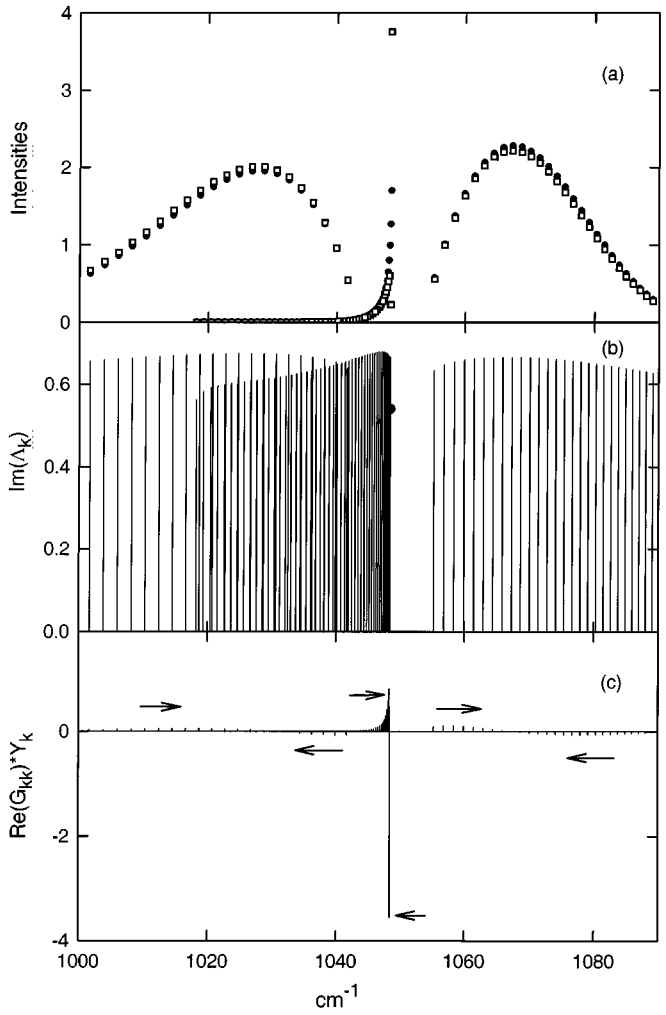

Fig. 6. Line parameters for the effective lines of the $K = 3$ sub-band as a function of line positions $\mathrm{Re}(\Lambda_k)$ (cf. Eq. (13)) for the helium pressure of 10 bars. (a) Comparison of the effective intensities in $\mathrm{cm}^{-2}\,\mathrm{atm}^{-1}$ (open squares) to the standard ones (given by Eq. (12)) valid for isolated lines used for the Lorentzian prediction (solid circles). (b) Half-widths (in $10^{-3}\,\mathrm{cm}^{-1}\,\mathrm{atm}^{-1}$). Note the point associated to the most intense line. (c) Distribution of the dispersive contributions. The arrows indicate the transfer of the intensity.

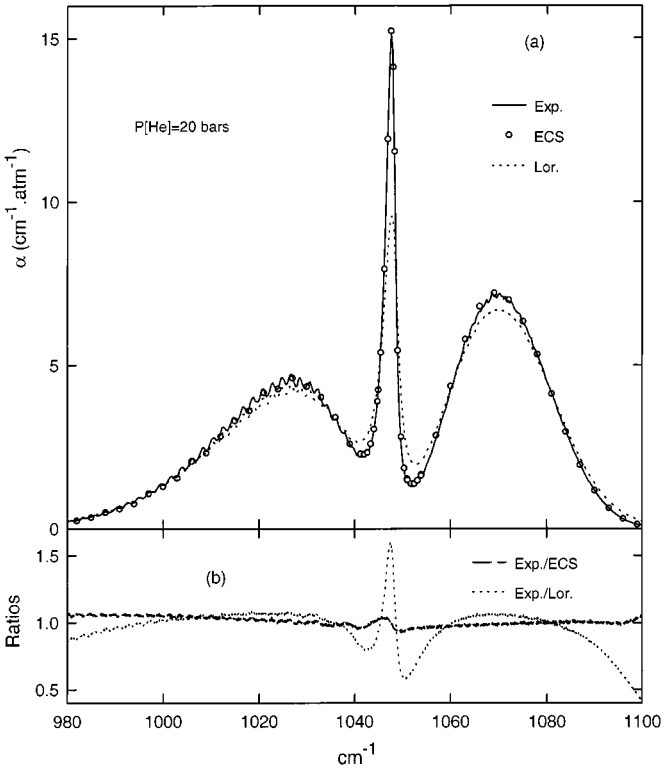

Fig. 7. Same as for Figure 4 with the helium pressure of 20 bars.

At greater pressures, the differences between an ECS calculation and a Lorentzian one are enhanced: see Figure 5. The rotational structure persists in the P and R branch regions, being completely washed out in the Q branches region. The ECS prediction accounts satisfactorily for the experiment over the entire profile in contrast with the IOS approximation which provides an excess of intensity transfer.

In order to follow the evolution of the band profile with helium pressure it may be of some interest to present a distribution of ECS calculated parameters of the effective lines (Eqs. (13-15)) for the most intense sub-band at $K = 3$.

Figure 6 gives intensities $\mathrm{Re}(G_{kk})$, half-widths $\mathrm{Im}(\Lambda_k)$ and products $\mathrm{Re}(G_{kk})Y_k = \mathrm{Im}(G_{kk})$ *versus* line positions $\mathrm{Re}(\Lambda_k)$. In Figure 6a the intensities are compared with the standard ones deduced from the work of Papousek *et al.* [18] and Lepere *et al.* [19]; they were used for the calculations of Lorentzian band shapes (Eq. (12)). This figure shows that the positions of lines are quite similar as well as intensities in the P and R branches, the only differences appearing for the first Q lines. The most intense Q line ($Q(3)$, cf. Fig. 6a) has the smallest linewidth (Fig. 6b), and it has a large negative interference parameter Y_k resulting in a strong dispersive component $\mathrm{Re}(G_{kk})Y_k$ (cf. Fig. 6c). This negative product and the dispersive contribution of the R lines account for the strong sub-Lorentzian behaviour of the absorption in the troughs between the Q and R branches (see Fig. 5). Similarly, such products for the other Q lines are responsible for the enhancement (the collisional narrowing) of the Q branches and, taking into account the dispersive contribution of the P lines, the sub-Lorentzian behaviour of the absorption in the troughs between the P and Q branches. The arrows in Figure 6c indicate these transfers of intensity inside the band.

Up to 20 bars the ECS calculation gives a fairly good agreement with the experimental spectrum over the entire band; see Figure 7. At higher pressures the situation becomes more complicated: see Figures 8 and 9. It is worth noting that the agreement remains satisfactory at the top of the Q branches region, but it is not the case for the troughs in the intermediate P-Q and Q-R regions, especially at 90 bars. It is known that these regions are particularly sensitive to interbranch coupling: see, for instance, reference [17] for the present case. These results may be

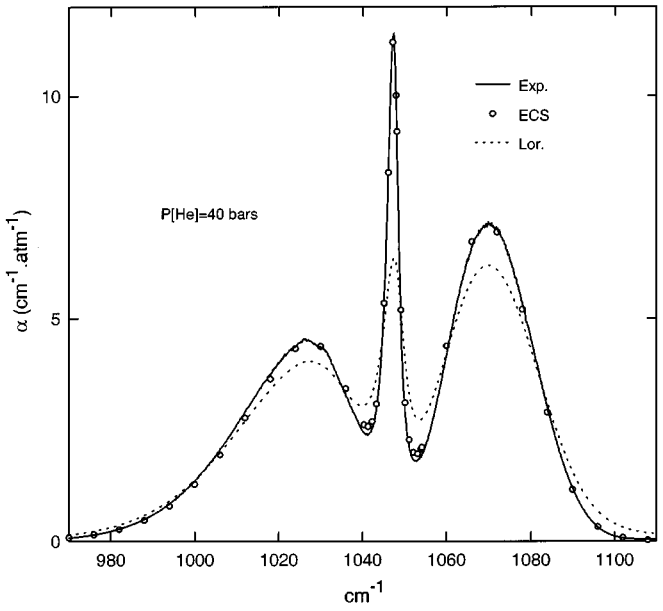

Fig. 8. Comparison between the measured spectrum (solid line), the Lorentz band profile (dotted line), and the ECS calculated profile (open circles) at the helium pressure of 40 bars.

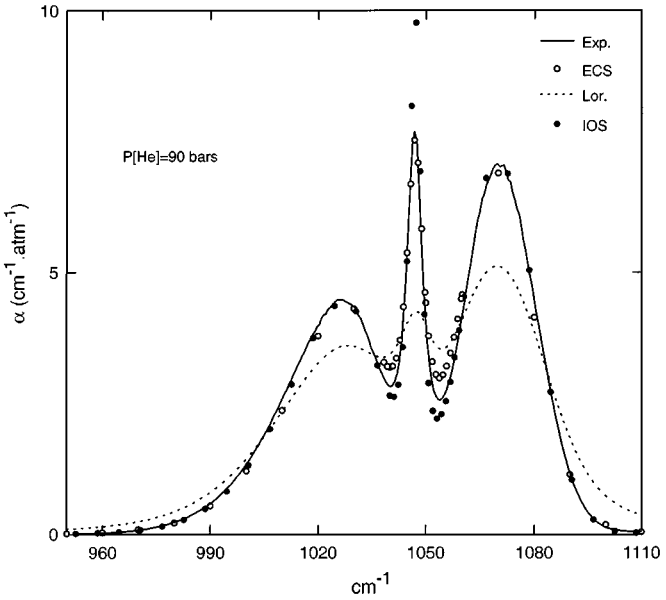

Fig. 9. Comparison between the experimental spectrum (solid line), the Lorentz band shape (dotted line), the ECS calculated profile (open circles) and the IOS calculated profile (solid circles) at the helium pressure of 90 bars.

due to some inaccuracy in the interbranch mixing cross-sections. Recall that our fitting procedure favoured the linewidths against only three experimental points of the spectrum at 10 bars. At any rate, it demonstrates that the role and the peculiarities of interbranch coupling should be studied in more detail.

The phenomena represented in Figure 6 are strengthened at 90 bars as is illustrated by Figure 10. The strong deviation from a Lorentzian spectrum shown in Figure 9

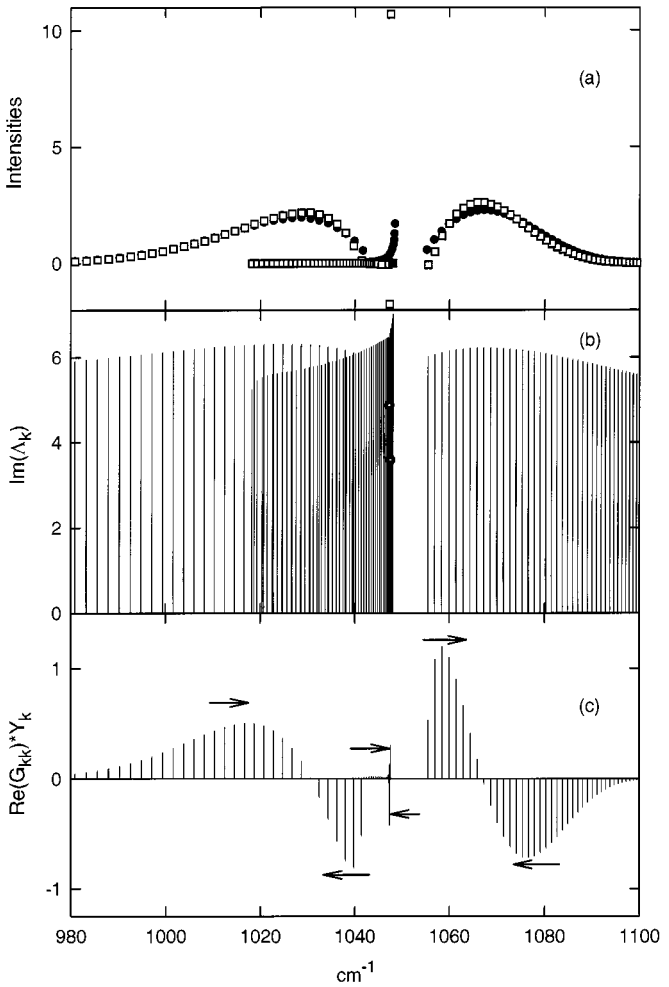

Fig. 10. Same as Figure 6 for the helium pressure of 90 bars. Note in (b) the points associated to the most intense lines.

is made evident in Figure 10a. This deviation appears not only in the Q branches region but also in the wings of the P and R branches. The Q branch is rather collapsed: its description is nearly reduced to a pair of lines. Their effective intensities appear to be of opposite signs, the positive one being 6 times as big as the negative one. Their half-widths are smaller than those of an isolated line, see Figure 10b, and the dispersive contributions of opposite signs (Fig. 10c) account for the broadening of the Q branch. Moreover, Figure 10c shows clearly the intensity redistribution in the P and R branches.

We should also mention that the IOS calculation departs more and more from the experimental spectrum as the pressure increases.

Finally, no shift or no relative shift of the P, Q and R branches (resulting of the superposition of all the K-sub-bands) has been observed, as is the case for instance for isotropic Raman Q branches at high pressure [45,46]. Therefore, no attempt has been done for the modeling of any pure vibrational dephasing.

6 Conclusion

The measured half-widths [11] have allowed us to attempt an ECS analysis of the ν_3 band shape of methyl fluoride. The calculated half-widths reproduce the main trends of the experimental ones. Unfortunately there are no measurements at higher J values since it is not easy to take into account small intensities of the lines, possible influence of some other bands, and a greater extent of line overlapping for $J = 20 \ldots 30$ in the ν_3 band. Nevertheless, the present study corroborates, in comparison with reference [17], the description of line mixing in the ν_3 band of CH_3F perturbed by helium within the framework of a more sophisticated rotational relaxation model.

The well-known ability of the ECS model to match band spectra of linear molecules has been confirmed for a symmetric top molecule even with some simplifications introduced. We have also attempted the above analysis using the IOS scaling law. The accuracy of the IOS approximation for higher rotational levels is easily improved by introducing simple corrections suggested by the ECS scheme: this procedure gives better behaviour for the linewidths and better agreement with experimental profiles. As was mentioned for other band shape analyses [43], the ECS model has demonstrated its superiority over the IOS one. Nevertheless, this point was not obvious at the beginning of this study. Indeed, Everitt and De Lucia [21] had found no improvement with respect to IOSA by using the ECS formalism to model the state-to-state rates for CH_3F-CH_3F collisions; if the IOS approximation were sufficient for this sort of interaction, it would be *a fortiori* sufficient for the CH_3F-He case.

The results presented here are somewhat different from those obtained by Everitt *et al.* [21]. Our experimental band shapes are related to the energy relaxation via the time evolution of a tensor of first rank, and we find that the additional parameter introduced in the framework of the ECS approximation is essential to achieve good agreement between calculated and experimental data, both for linewidths and for selected regions on the band shape sensible to line mixing. In fact, we obtain the diagonal matrix elements applying the sum rules for the relaxation matrix to the calculated set of the non-diagonal ones (see Eq. (10)), and this feature of the relaxation matrix was not considered in reference [21]. In our opinion, the data set of reference [21] may not be particularly sensitive to the adiabaticity level ruled by the ECS scaling law, contrary to our case, since Everitt *et al.* [21] only consider low rotational states and small ΔJ values ($\Delta J \leq 10$).

It would be interesting to compare the present results with the model of Filippov *et al.* [16,17] and, in particular, to investigate in more detail the role of interbranch coupling: this will be done in a forthcoming paper.

This work was supported in part by the Russian Foundation for Basic Research (Grant No. 97-03-33655a). We also thank C.Boulet and J.M. Hartmann (Laboratoire de Physique Moléculaire et Applications, Orsay) for helpful discussions.

References

1. A. Lévy, N. Lacome, C.C. Chackerian Jr., *Collisional Line Mixing in Spectroscopy of the Earth's Atmosphere and Interstellar Medium*, edited by K.N. Rao, A. Weber (Academic Press, New York, 1992).
2. S. Green, *Calculation of Pressure Broadened Spectral Line Shapes Including Collisional Transfer of Intensity,* in *Status and Future Developments in Transport Properties*, edited by W.A. Wakeham (Kluwer Academic, Dordrecht, 1992).
3. J. Boissoles, F. Thibault, C. Boulet, J. Quant. Spectrosc. Radiat. Transfer **56**, 835 (1996).
4. R. Rodrigues, G. Blanquet, J. Walrand, B. Khalil, R. Le Doucen, F. Thibault, J.M. Hartmann, J. Mol. Spectrosc. **186**, 256 (1997); J.P. Bouanich, R. Rodrigues, J.M. Hartmann, J.L. Domenech, D. Bermejo, *ibid.* **186**, 269 (1997).
5. F. Thibault, J. Boissoles, C. Boulet, L. Ozanne, J.P. Bouanich, C.F. Roche, J.M. Hutson, J. Chem. Phys. **109**, 6338 (1998).
6. G. Blanquet, P. Coupe, J. Walrand, J.P. Bouanich, J. Quant. Spectrosc. Radiat. Transfer **51**, 671 (1994).
7. G. Blanquet, J. Walrand, J.C. Populaire, J.P. Bouanich, J. Quant. Spectrosc. Radiat. Transfer **53**, 211 (1995).
8. M. Fabian, F. Ito, K.M.T. Yamada, J. Mol. Spectrosc. **173**, 591 (1995).
9. B. Lance, M. Lepère, G. Blanquet, J. Walrand, J.P. Bouanich, J. Mol. Spectrosc. **180**, 100 (1996).
10. K. Jacquiez, G. Blanquet, J. Walrand, J.P. Bouanich, J. Mol. Spectrosc. **175**, 386 (1996).
11. I.M. Grigoriev, J.P. Bouanich, G. Blanquet, J. Walrand, M. Lepère, J. Mol. Spectrosc. **186**, 48 (1997).
12. D.R. Wiley, R.E. Timlin, P.G. DeNardo, P.L. Null, P.L. Pondillo, T. Tyszka, J. Chem. Phys. **107**, 8252 (1997).
13. Ph. Brechignac, J. Chem. Phys. **76**, 3389 (1982).
14. J.M. Hartmann, C. Boulet, M. Margottin-Maclou, F. Rachet, B. Khalil, F. Thibault, J. Boissoles, J. Quant. Spectrosc. Radiat. Transfer **54**, 705 (1995); J.M. Hartmann, J.P. Bouanich, G. Blanquet, J. Walrand, N. Lacome, *ibid* **54**, 723 (1995); G. Blanquet, J. Walrand, J.M. Hartmann, J.P. Bouanich, *ibid.* **55**, 289 (1996).
15. R. Rodrigues, P. De Natale, G. Di Lonardo, J.M. Hartmann, J. Mol. Spectrosc. **175**, 429 (1996).
16. M.V. Tonkov, N.N. Filippov, Yu.M. Timofeyev, A.V. Polyakov, J. Quant. Spectrosc. Radiat. Transfer **56**, 783 (1996).
17. I.M. Grigoriev, R. Le Doucen, A. Benidar, N.N. Filippov, M.V. Tonkov, J. Quant. Spectrosc. Radiat. Transfer **58**, 287 (1997).
18. D. Papousek, R. Tesar, P. Pracna, J. Kauppinen, S.P. Belov, M.Yu. Tretyakov, J. Mol. Spectrosc. **146**, 127 (1991); D. Papousek, J.F. Ogilvie, S. Civis, M. Winnewisser, *ibid.* **149**, 109 (1991); D. Papousek, Z. Papouskova, J.F. Ogilvie, P. Pracna, S. Civis, M. Winnewisser, *ibid.* **153**, 145 (1992).
19. M. Lepère, G. Blanquet, J. Walrand, J. Mol. Spectrosc. **177**, 307 (1996) and Spectrochim. Acta A **52**, 1029 (1996).
20. D. Robert, L. Bonamy, J. Phys. (Paris) **40**, 923 (1979).
21. H.O. Everitt, F.C. De Lucia, J. Chem. Phys. **92**, 6480 (1990).
22. M.M. Beaky, D.C. Flatin, J.J. Holton, T.M. Goyette, F.C. De Lucia, J. Mol. Struct. **352/353**, 245 (1995).

23. D.R. Wiley, T.M. Goyette, W.L. Ebenstein, D.N. Bittner, F.C. De Lucia, J. Chem. Phys. **91**, 122 (1989).
24. D.R. Wiley, V.-E.Choong, J.P. Goodelle, K.A. Ross, J. Chem. Phys. **97**, 4723 (1992).
25. S. Green, J. Chem. Phys. **70**, 816 (1979).
26. R. Le Doucen, C. Boulet, Spectrochim. Acta A **51**, 1239 (1995).
27. M.H. Alexander, J. Chem. Phys. **77**, 1860 (1982).
28. U. Shin, R.H. Schwendeman, J. Chem. Phys. **94**, 7560 (1991); U. Shin, Q. Song, R.H. Schwendeman, J. Chem. Phys. **95**, 3964 (1991).
29. G.C.M. Van Der Sanden, P.E.S. Wormer, A. Van der Avoird, J. Schleipen, J.J. ter Meulen, J. Chem. Phys. **97**, 6460 (1992); G.C.M. Van Der Sanden, P.E.S. Wormer, A. Van der Avoird, *ibid.* **105**, 3079 (1996).
30. D. Harradine, B. Foy, L. Laux, M. Dubs, J.I. Steinfeld, J. Chem. Phys. **81**, 4267 (1984).
31. T. Oka, *Advances in Atomic and Molecular Physics*, edited by D.R. Bates, I. Estermann, Vol. 9 (Academic Press, 1973).
32. A.E. DePristo, R. Ramaswamy, S.D. Augustin, H. Rabitz, J. Chem. Phys. **71**, 850 (1979).
33. L. Bonamy, J.M. Huet, J. Bonamy, D. Robert, J. Chem. Phys. **95**, 3361 (1991).
34. R.G. Gordon, R.P. Mc Ginnis, J. Chem. Phys. **49**, 2455 (1968).
35. P.W. Rosenkranz, IEEE Trans. Anten. Propag. **23**, 498 (1975).
36. K.S. Lam, J. Quant. Spectrosc. Radiat. Transfer **17**, 351 (1977).
37. E.W. Smith, J. Chem. Phys. **74**, 6658 (1981).
38. M.O. Bulanin, A.B. Dokuchaev, M.V. Tonkov, N.N. Filippov, J. Quant. Spectrosc. Radiat. Transfer **31**, 521 (1984).
39. L. Bonamy, F. Emond , Phys. Rev. A **51**, 1235 (1995).
40. B. Lavorel, G. Millot, R. Saint-Loup, H. Berger, L. Bonamy, J. Bonamy, D. Robert, J. Chem. Phys. **93**, 2176 (1990).
41. J. Boissoles, F. Thibault, R. Le Doucen, V. Menoux, C. Boulet, J. Chem. Phys. **101**, 6552 (1994).
42. R.T. Pack, J. Chem. Phys. **70**, 3424 (1979).
43. J. Boissoles, F. Thibault, R. Le Doucen, V. Menoux, C. Boulet, J. Chem. Phys. **100**, 215 (1994).
44. C. Roche, A. Ernesti, J.M. Hutson, A.S. Dickinson, J. Chem. Phys. **104**, 2156 (1996).
45. B. Lavorel, G. Millot, G. Fanjoux, R. Saint-Loup, J. Chem. Phys. **101**, 174 (1994).
46. Yu.I. Bulgakov, M.L. Strekalov, Opt. Spectrosc. **76**, 516 (1994).